

## NUMERICAL INVESTIGATION ON LIQUID HYDRAZINE BEHAVIOUR DURING VENTING INTO SPACE

P. Reynier <sup>†</sup>, P. Wesseling<sup>\*</sup>, L. Marraffa<sup>†</sup> and D. Giordano<sup>†</sup>

<sup>†</sup> Propulsion and Aerothermodynamics Division, ESA/ESTEC, PO Box 299, 2200 AG Noordwijk AZ, The Netherlands, e-mail: lmarraf@estec.esa.nl, web page: <http://www.estec.esa.nl/>

<sup>\*</sup> Faculty of Technical Mathematics and Informatics, Delft University of Technology, PO Box 5031, 2600 GA Delft, The Netherlands, e-mail: p.wesseling@twi.tudelft.nl, web page: <http://dutita0.twi.tudelft.nl/>

**Key words:** liquid depressurization, venting, hydrazine, two-phase flow, staggered scheme, thermodynamic model.

**Abstract.** *A numerical method (pressure-correction method using a staggered grid) is coupled to a two-phase thermodynamic model for hydrazine. The thermodynamic model accounts for the compressibility of the liquid and the same state equation is used for liquid and vapour. This approach is applied to the numerical predictions of liquid hydrazine venting. During this process the liquid hydrazine undergoes a strong depressurization. When the pressure reaches the saturation pressure vaporization occurs. This phenomenon takes place near the outlet and induces variations of temperature which could cause ice formation and pipe clogging. In order to assess the risk of clogging, numerical simulations of the venting line have been performed using a quasi one-dimensional approach. The pressure-correction method is well-suited to the simulation of compressible flows of fluids with nonconvex equation of state at the low Mach numbers that occur during hydrazine venting. The numerical results have been validated using experimental data and have given an estimate of the clogging risk.*

## 1 INTRODUCTION

The study of tank venting through a discharge line with liquid flashing is of high interest in many industrial processes. This kind of flow occurs in the automotive and aeronautical industries (e.g. Zeigerson-Katz and Sher [1]), where insight in this process is essential for improving the fuel injection process. The same type of flow concerns also the technological hazards associated with the loss of containment of liquefied gases (e.g. Curtelin [2], Veneau [3] and Hervieu and Veneau [4]).

The venting of propellant vessels is of major interest for space applications. This process is encountered in rockets, spacecraft and satellites. The first study found in the literature devoted to this topic has been published by Neher [5], and concerned the venting of tank propellant in the parking orbit of the Saturn S-IVB rocket. Since then, many numerical and experimental investigations have been focused on different aspects of space venting. Examples are the investigations on the venting of water from the shuttle conducted by Pike et al. [6] and Kofski et al. [7].

In the framework of the Ariane 5 project, the venting process is of major interest. At the end of the launch of Ariane 5, the rocket is passivated. The passivation includes the venting into space of all the propellants stored in tanks. This process is performed to avoid the explosion risks due to solar heating, micrometeorite impact or reentry heating. An explosion would cause the undesirable production of stable debris in space. The present study concerns the passivation of the attitude control system called SCA (French acronym for "Système de Contrôle d'Attitude"), which is performed at 1000 km altitude. The venting of liquid hydrazine into space through a discharge line is required. The liquid hydrazine is stored in tanks at a pressure between 6 and 25 bar. When the tanks are vented, the liquid undergoes a large pressure drop (until vacuum pressure). Due to the pressure decrease along the vent line, the hydrazine begins to boil. Then, changes in the temperature may produce ice near the exit. The presence of ice could provoke pipe clogging and therefore a risk of explosion. In order to avoid this risk, the location of phase changes and temperature distribution along the vent line and especially near the exit need to be investigated to ensure the success of the venting process.

The present study is focused on the simulation of liquid depressurization. To predict the liquid behaviour, a quasi one-dimensional approach has been chosen with a two-phase thermodynamic model for hydrazine. This model has been developed by Giordano and De Serio [8] in agreement with thermodynamic theory and has been validated using the experimental data available in the literature. This nonlinear model is able to predict the thermodynamic behaviour of hydrazine from high pressure until vaporization accounting for the liquid compressibility. The originality of this work from the numerical point of view is the simulation of compressible flows at low Mach numbers using this nonlinear model.

The flow to be simulated has a low velocity and a low Mach number,  $Ma < 0.03$ , and is submitted to a strong pressure drop. Therefore, the numerical method chosen has to

be able to simulate flows at low Mach numbers and to be stable when flows are computed using a thermodynamic model for a compressible liquid. In fact the method has to be able to solve a compressible flow in the limit of  $Ma \rightarrow 0$ . Several alternatives are possible:

- Standard compressible methods cannot be used because severe convergence problems can occur as  $Ma \rightarrow 0$ . For incompressible flows, density and pressure are independent, so the pressure cannot be calculated from the density. For this reason density-based methods fail. But compressible methods can be adapted to fairly low Mach numbers by introducing preconditioning but time accuracy is lost.

- Asymptotic methods based on expansion of variables in Mach number series. But the Mach number has to be uniformly low to ensure accuracy.

- Incompressible methods extended to compressible flows, Bijl and Wesseling [9], among others, have developed this method. This results in a unified method for incompressible and compressible flows with accuracy and efficiency uniform in the Mach number.

The last method has been selected for this study. The scheme is designed such that for  $Ma \rightarrow 0$  the classical incompressible method of Harlow and Welch [10] is recovered. Perfect gas or nonconvex equations of state can be incorporated without problem. In this paper this numerical method is applied to the flow simulation using the thermodynamic model proposed by Giordano and De Serio [8]. The numerical results are validated using the experimental data obtained by Foucaud [11] and the clogging risk is estimated.

## 2 GOVERNING EQUATIONS

The equations to be solved are the conservation laws for mass and momentum and the transport equation for the internal energy. A thermodynamic model has to be used to close the set of equations. The mass and momentum conservation equations can be written in the following form, where  $A$  is the area of the cross-section,  $D$  the pipe diameter,  $\rho$  the density,  $P$  the pressure and  $U$  the velocity:

$$\frac{\partial \rho}{\partial t} + \frac{1}{A} \frac{\partial}{\partial x} \rho A U = 0 \quad (1)$$

$$\frac{\partial}{\partial t} \rho U + \frac{1}{A} \frac{\partial}{\partial x} (\rho A U^2) + \frac{\partial P}{\partial x} + \frac{2C_f}{D} \rho U^2 - \rho g = 0 \quad (2)$$

The gravity term  $\rho g$  is included, because we will compare computations with a ground test on a vertical pipe. The value of  $g$  is  $9.81 \text{ m.s}^{-2}$ .

For two-phase flows the friction coefficient is given by:

$$C_f = C_{f.sp} \Phi^2 \quad (3)$$

$C_{f.sp}$  is the friction coefficient for a liquid flow computed using the explicit formulae proposed by Jain [12]. At the area change the same treatment as the one used by Reynier

et al [13] has been applied.  $\Phi^2$  is deducted from the correlation of Lockart-Martinelli modified by Richardson (see Veneau [3]):

$$\Phi^2 = (1 - \alpha)^{-1.75} \quad (4)$$

where  $\alpha$  is the void fraction related to the dryness fraction  $\chi$  by the following relation:

$$\alpha = \chi \frac{\rho}{\rho_V^s} \quad (5)$$

where  $\rho_V^s$  is the vapour density at saturation.

Due to the pressure correction method it is not possible to solve directly the conservative equation for the total energy. Therefore, the transport equation for the internal energy  $e$  is solved. This equation is given by:

$$\frac{\partial e}{\partial t} + U \frac{\partial e}{\partial x} + \frac{P}{A\rho} \frac{\partial AU}{\partial x} - \frac{2C_f}{D} U^3 = 0 \quad (6)$$

### 3 THERMODYNAMIC MODEL

The thermodynamic model used for hydrazine has been developed by Giordano and De Serio [8]. It accounts for the compressibility of the liquid and liquid-vapour phase change. The equation of state is compatible for liquid and vapour. This model consists of an equation of state and an equation for the internal energy. At saturation, the pressure is a function of temperature. The equation of state is given by:

$$P = \frac{RT}{v - a} - \frac{c}{T^{n_e}(v + b)^2} \quad (7)$$

where  $T$  is the temperature and  $v = 1/\rho$  the specific volume. At saturation  $v$  is equal to the specific volume of the liquid  $v_l^s$  or to the specific volume of the vapour  $v_v^s$ . The value of  $n_e$  used for the calculations is 0.7. The constant  $R$  is equal to  $R_G/M_{N_2H_4}$  where  $R_G$  is the constant for a perfect gas equal to 8.314 J/K and  $M_{N_2H_4} = 32.04510^{-3}$ kg is the molar mass of hydrazine. The constants a, b, c are given by the following relations:

$$a = v_c \left( 1 - \frac{1}{4L_c} \right) \quad (8)$$

$$b = v_c \left( \frac{3}{8L_c - 1} \right) \quad (9)$$

$$c = \frac{27}{64} \frac{R^2 T_c^{n_e+2}}{P_c} \quad (10)$$

where  $L_c = P_c v_c / RT_c$ .  $P_c$ ,  $v_c$ ,  $T_c$  are respectively the pressure, the volume and the temperature of hydrazine at the critical point. Their values have been given by Giordano and

De Serio [8] and are:  $P_c = 147$  bar,  $v_c = 3.7410^{-3}$  m<sup>3</sup>/kg and  $T_c = 653.15$  K.

Another equation is needed for the internal energy. This equation is given by:

$$e = K_2 + \int \Phi(T)dT - \frac{c(n_e + 1)}{T^{n_e}} \sum_{l,v} \frac{\chi_i}{(v_i + b)} \quad (11)$$

where  $K_2 = 11RT_c$ .  $\chi_i$  is the fraction of liquid and vapour defined as:

$$v = \chi_l v_l + \chi_v v_v \quad (12)$$

with,  $\chi_v + \chi_l = 1$ .

The integral  $\int \Phi(T)$  is approximated by the following series:

$$\int \Phi(T)dT = \sum_{k=1}^7 \frac{A_k}{k} \left(\frac{T}{T_c}\right)^k \quad (13)$$

where the coefficients  $A_k$  are listed in table 1.

A <sub>1</sub>	3.3083	B <sub>1</sub>	9.9677 10 <sup>-3</sup>
A <sub>2</sub>	9.5779	B <sub>2</sub>	0.2416
A <sub>3</sub>	-42.7878	B <sub>3</sub>	-2.9151
A <sub>4</sub>	1.4352 10 <sup>2</sup>	B <sub>4</sub>	11.3201
A <sub>5</sub>	-2.0802 10 <sup>2</sup>	B <sub>5</sub>	-18.9928
A <sub>6</sub>	1.3905 10 <sup>2</sup>	B <sub>6</sub>	11.8671
A <sub>7</sub>	-35.8884		

Table 1: Values of  $A_k$  and  $B_k$  obtained by fitting of experimental data (see Giordano and De Serio [8])

The saturation pressure is given by the following equation, established by Giordano and De Serio [8] using interpolation of experimental data:

$$P_{sat}(T) = P_c \sum_{k=1}^6 B_k \left(\frac{T}{T_c}\right)^{k-1} \quad (14)$$

where the coefficients  $B_k$  are given in table 1. The relation (14) is valid for the range of temperature occurring in our application.

The specific volumes for liquid,  $v_l^s$ , and vapour,  $v_v^s$ , at saturation are given by the following relations:

$$\frac{v_c}{v_l^s(T)} = \sum_{k=0}^8 C_k^1 \left(\frac{T}{T_c}\right)^k \quad (15)$$

$C_0^1$	$-8.1950 \cdot 10^1$	$C_0^2$	$-4.0914 \cdot 10^{-2}$
$C_1^1$	$1.2887 \cdot 10^3$	$C_1^2$	$4.0628 \cdot 10^{-1}$
$C_2^1$	$-8.2248 \cdot 10^3$	$C_2^2$	$-1.1402$
$C_3^1$	$2.9272 \cdot 10^4$	$C_3^2$	$-1.0532$
$C_4^1$	$-6.3648 \cdot 10^4$	$C_4^2$	$1.0012 \cdot 10^1$
$C_5^1$	$8.6622 \cdot 10^4$	$C_5^2$	$-9.8820$
$C_6^1$	$-7.2123 \cdot 10^4$	$C_6^2$	$-2.1992 \cdot 10^1$
$C_7^1$	$3.3623 \cdot 10^4$	$C_7^2$	$4.8736 \cdot 10^1$
$C_8^1$	$-6.7275 \cdot 10^3$	$C_8^2$	$-2.5375 \cdot 10^1$

Table 2: Values of  $C_k^1$  and  $C_k^2$  given by Giordano and De Serio [8]

$$\frac{v_c}{v_v^s(T)} = \sum_{k=0}^8 C_k^2 \left(\frac{T}{T_c}\right)^k \quad (16)$$

where the coefficients  $C_k^1$  and  $C_k^2$  are listed in table 2.

#### 4 TWO-PHASE MODELLING

For the two-phase modelling of the flow, the hypothesis of a small void fraction has been done. Therefore, the mechanical effects between the two phases are neglected. According to Bilicki et al [14], this assumption seems to be justified for bubbly flows with a void fraction,  $\alpha \leq 0.05$ . For higher void fraction, transition from bubbly to churn flow takes place. According to Minemura et al [15], this transition occurs in the range  $0.08 < \alpha < 0.14$ . In churn flows, mechanical effects become important and cannot be neglected. As a consequence, a mixture model cannot be applied to the prediction of churn flows. In the present case, the single-phase calculations indicate that the physical conditions for vaporization are reached near the exit. Therefore, the hypothesis of a bubbly flow has been adopted and the two-phase computations have been performed using a mixture model.

One of the most famous mixture model is the homogeneous relaxation model (HRM) developed by Bilicki et al [16, 14]. The predictions of Veneau [3] showed the superiority of this model compared to the other mixture models. Since our application is close to the flashing flow investigated by Veneau [3], the HRM model has been chosen for the two-phase calculations.

In the HRM model it is assumed that the effects of vaporization and condensation are significant. The liquid is considered to be superheated while the vapour is in the state of equilibrium at the saturation temperature. In this model the thermodynamic non-equilibrium is taken into account through a relaxation time and an equation is solved for the dryness fraction. The equation for the dryness fraction has the following form:

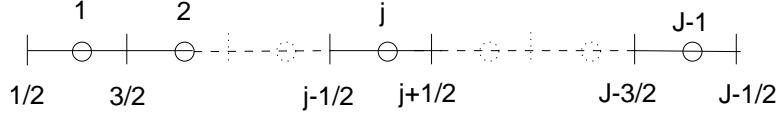


Figure 1: Staggered grid used for the one-dimensional predictions, here the grid is uniform

$$\frac{\partial \chi}{\partial t} + U \frac{\partial \chi}{\partial x} + \frac{\chi - \bar{\chi}}{\theta_\chi} = 0 \quad (17)$$

The relaxation time,  $\theta_\chi$ , is an additional function depending on the thermodynamic state of the system and should be defined by a separate equation. The relaxation corresponds to the transition of the thermodynamic system from nonequilibrium to equilibrium. During this transition bubble growth occurs. The initial growth of the bubble nucleus depends strongly on the interfacial mechanical interactions like acceleration, pressure forces and surface tension forces. During this stage, thermal phenomena like heat transfer and phase change are negligible. As the nucleus radius increases, the bubble growth becomes mostly dependent on heat supply that is consumed to vaporize the liquid on the bubble surface. Therefore, a realistic prediction of flashing flows requires to take into account the thermodynamic nonequilibrium between the phases. In the present study no experimental data are available for hydrazine to establish the function  $\theta_\chi$ . Hence, like in the computations of water depressurization made by Bilicki et al [14], a constant has been used. This value has been chosen equal to 2.

## 5 NUMERICAL METHOD

The numerical method is a finite-volume scheme that uses a staggered grid, therefore no measures have to be taken to avoid spurious pressure oscillations. The scheme is simple, due to the choice of primitive variables:  $\rho$ ,  $m = \rho U$ ,  $\chi$  and  $e$ , and the use of a staggered grid.

## 5.1 Discretisation in time and space

The set of equations presented in §2 is discretised on a staggered grid. The computational domain  $(0,L)$  is divided in cells  $\Omega_j$ ,  $j=1..J-1$  of possibly non-uniform size  $\Delta x_j$ . The center of  $\Omega_j$  is denoted by  $x_j$  and its two end points are denoted by  $x_{j\pm 1/2}$ . The thermodynamic variables,  $P$ ,  $\rho$ ,  $\chi$  and  $e$ , are located in  $x_j$ . The dynamic variables  $U$  and  $m = \rho U$  are located in  $x_{j\pm 1/2}$ .  $A_j$  is the cross section area at the point  $x_j$  and  $A_{j+1/2}$  is the cross section area at the point  $x_{j+1/2}$ . The mesh is represented in figure 1.

The following notations are used:

$$\begin{aligned}\delta e_j &= e_j^{n+1} - e_j^n; \\ \delta \rho_j &= \rho_j^{n+1} - \rho_j^n; \\ \delta P_j &= P_j^{n+1} - P_j^n; \\ \lambda_j &= \frac{\Delta t}{\Delta x_j}, \lambda_{j+1/2} = \frac{2\Delta t}{\Delta x_j + \Delta x_{j+1}}.\end{aligned}$$

A non-uniform mesh is used in order to allow mesh refinement near the end of the pipe, where the change of the cross-section is abrupt. For the discretisation in time, a first order explicit/implicit Euler method is used. An upwind discretisation has been chosen for the convective terms in the internal energy, dryness and momentum equations. The scheme is defined as follows:

$$\rho_j^{n+1} - \rho_j^n + \frac{\lambda_j}{A_j} (Am^{n+1})|_{j-1/2}^{j+1/2} = 0 \quad (18)$$

$$\begin{aligned}m_{j+1/2}^{n+1} - m_{j+1/2}^n + \frac{\lambda_{j+1/2}}{A_{j+1/2}} (Am^n U^n)|_j^{j+1} + \lambda_{j+1/2} P^{n+1}|_j^{j+1} \\ + \Delta t \left( \frac{2C_f}{D_{j+1/2}} (Um)_{j+1/2}^n - \rho_{j+1/2}^n g \right) = 0\end{aligned} \quad (19)$$

$\rho_{j+1/2}$  is computed using an interpolation between the two neighbouring points.

For the energy equation the discretisation is fully explicit:

$$e_j^{n+1} - e_j^n + \lambda_j U_j^n e^n|_{j-1/2}^{j+1/2} + \frac{\lambda_j P_j^n}{A_j \rho_j^n} (AU^n)|_{j-1/2}^{j+1/2} - \Delta t \frac{2C_f}{D_j} (U_j^n)^3 = 0 \quad (20)$$

The velocity at the center of the cells is computed by interpolation of the velocities at the two neighbouring points.

The dryness fraction is computed at the pressure points. An implicit formulation for the relaxation term is used:

$$\chi_j^{n+1} - \chi_j^n + \lambda_j U_j^n \chi^n|_{j-1/2}^{j+1/2} + \Delta t \frac{\chi_j^{n+1} - \bar{\chi}_j^{n+1}}{\theta_\chi} = 0 \quad (21)$$

## 5.2 Boundary Conditions

The following boundary conditions are used for the one-dimensional flow in a pipe.  $T_{\text{left}}$ ,  $\chi_{\text{left}}$  and  $m_{\text{left}}$  are given at the inlet. At the outlet,  $P_{\text{right}}$  is prescribed. For single-phase computations it is equal to 1 mbar, for two-phase predictions the saturation pressure of the spray at equilibrium measured at ONERA by Foucault[11] is chosen.

- Dryness fraction

At the inlet: The fluid is supposed to be a liquid,

$$\chi_1 = \chi_{\text{left}} = 0 \quad (22)$$

At the outlet:

$$\chi_{J-1}^{n+1} = \chi_{J-1}^n - \lambda_{J-1} U_{J-1}^n (\chi_{J-1}^n - \chi_{J-2}^n) - \Delta t \frac{\chi_{J-1}^{n+1} - \bar{\chi}_{J-1}^{n+1}}{\theta_\chi} \quad (23)$$

- Internal energy

At the inlet:

$$e_1 = e(T_{\text{left}}, \rho_{\text{left}}) \quad (24)$$

where  $\rho_{\text{left}}$  is calculated using the state equation:

$$\rho_{\text{left}} \approx f(T_{\text{left}}, P_1) \quad (25)$$

where  $P_1$  is the pressure obtained at the preceding time step.

At the outlet a boundary condition for the internal energy is not given and not required by the first order upwind scheme, which takes the following form near the outlet:

$$e_{J-1}^{n+1} = e_{J-1}^n - \lambda_{J-1} U_{J-1}^n (e_{J-1}^n - e_{J-2}^n) - \frac{\lambda_{J-1} P_{J-1}^n}{A_{J-1} \rho_{J-1}^n} ((AU^n)_{J-1/2} - (AU^n)_{J-3/2}) + \Delta t \frac{2C_f}{D_{J-1}} (U_{J-1}^n)^3 \quad (26)$$

- Momentum:

At the inlet:

$$m_{1/2} = m_{\text{left}} \quad (27)$$

At the outlet: As for the internal energy an upwind scheme is used. The finite volume discretization of the momentum equation takes place by integration over a half cell ( $\lambda_{J-1/2} = 2\lambda_{J-1}$ ):

$$m_{J-1/2}^{n+1} = m_{J-1/2}^n - \frac{\lambda_{J-1/2}}{A_{J-1/2}} ((Am^n U^n)_{J-1/2} - (Am^n U^n)_{J-3/2}) + \lambda_{J-1/2} (P_{\text{right}} - P_{J-1}^{n+1}) - \Delta t \left( \frac{2C_f}{D_{J-1/2}} (mU)_{J-1/2}^n - \rho_{\text{right}} g \right) \quad (28)$$

where  $\rho_{\text{right}}$  is evaluated as:

$$\rho_{\text{right}} = \rho_{j-1}^n \quad (29)$$

### 5.3 Pressure-correction method

The system (18)-(21) is solved by an iterative method. The method consists of the following steps:

(1) Find  $e^{n+1}$  from (20) using the first order upwind scheme, assuming  $U > 0$ :

$$\begin{aligned} e_j^{n+1} = e_j^n - \lambda_{j-1/2} U_j^n (e_j^n - e_{j-1}^n) - \frac{\lambda_j P_j^n}{A_j \rho_j^n} ((AU^n)_{j+1/2} \\ - (AU^n)_{j-1/2}) + \Delta t \frac{2C_f}{D_j} (U_j^n)^3 \end{aligned} \quad (30)$$

(2) Momentum prediction step. Determine  $m^*$  from (19) using  $P^n$  instead of  $P^{n+1}$  and using the first order upwind scheme:

$$\begin{aligned} m_{j+1/2}^* = m_{j+1/2}^n - \frac{\lambda_j}{A_{j+1/2}} ((Am^n U^n)_{j+1/2} - (Am^n U^n)_{j-1/2}) \\ - \lambda_{j+1/2} (P_{j+1}^n - P_j^n) - \Delta t \left( \frac{2C_f}{D_{j+1/2}} (mU)_{j+1/2}^n - \rho_{j+1/2}^n g \right) \end{aligned} \quad (31)$$

(3) Pressure-correction step. Write,

$$m_{j+1/2}^{n+1} = m_{j+1/2}^* - \lambda_{j+1/2} \delta P |_j^{j+1} \quad (32)$$

At the outlet,  $P_{\text{right}}$  is imposed and  $\delta P_{\text{right}} = 0$ :

$$m_{J-1/2}^{n+1} = m_{J-1/2}^* + \lambda_{J-1/2} \delta P_{J-1} \quad (33)$$

An equation for  $\delta P_j$  and  $\delta \rho_j$  is found by substitution of (32) in the mass conservation equation.

$$\delta \rho_j + a_j \delta P_{j-1} + b_j \delta P_j + c_j \delta P_{j+1} = RHS(j) \quad (34)$$

The expressions for  $a_j, b_j, c_j$  are:

$$a_j = -\frac{\lambda_j}{A_j} \lambda_{j-1/2} A_{j-1/2} \quad (35)$$

$$b_j = \frac{\lambda_j}{A_j} (\lambda_{j-1/2} A_{j-1/2} + \lambda_{j+1/2} A_{j+1/2}) \quad (36)$$

$$c_j = -\frac{\lambda_j}{A_j} \lambda_{j+1/2} A_{j+1/2} \quad (37)$$

The expression of the right-hand-side term is:

$$RHS(j) = -\frac{\lambda_j}{A_j}((Am^*)_{j+1/2} - (Am^*)_{j-1/2}) \quad (38)$$

At the inlet the equation (34) becomes,

$$\delta\rho_1 - \frac{\lambda_1}{A_1}\lambda_{3/2}A_{3/2}(\delta P_2 - \delta P_1) = RHS(1) \quad (39)$$

Hence,

$$a_1 = 0 \quad (40)$$

$$b_1 = \frac{\lambda_1}{A_1}\lambda_{3/2}A_{3/2} \quad (41)$$

$$c_1 = -\frac{\lambda_1}{A_1}\lambda_{3/2}A_{3/2} \quad (42)$$

$$RHS(1) = -\frac{\lambda_1}{A_1}((Am^*)_{3/2} - (Am^*)_{1/2}) \quad (43)$$

The following expressions are obtained at the outlet:

$$a_{J-1} = -\frac{\lambda_{J-1}}{A_{J-1}}\lambda_{J-3/2}A_{J-3/2} \quad (44)$$

$$b_{J-1} = \frac{\lambda_{J-1}}{A_{j-1}}(\lambda_{J-1/2}A_{J-1/2} + \lambda_{J-3/2}A_{J-3/2}) \quad (45)$$

$$c_{J-1} = 0 \quad (46)$$

$$RHS(J-1) = -\frac{\lambda_{J-1}}{A_{J-1}}((Am^*)_{J-1/2} - (A\sigma^n m^*)_{J-3/2}) \quad (47)$$

Because  $\delta P$  depends nonlinearly on  $\delta\rho$  and  $\delta e$ , (34) is a nonlinear system for  $\delta P$ . It is solved in two substeps, as follows:

- First a rough approximation of  $\delta\rho$  is done using the values at the previous time step:

$$\delta\rho = \left(\frac{\partial\rho}{\partial e}\right)_{P,j}^n \delta e_j + \left(\frac{\partial\rho}{\partial P}\right)_{e,j}^n \delta P_j \quad (48)$$

The partial derivatives of  $\rho$  with respect to  $P$  and  $e$  come from the thermodynamic model (e.g. Reynier et al [13] [17]).

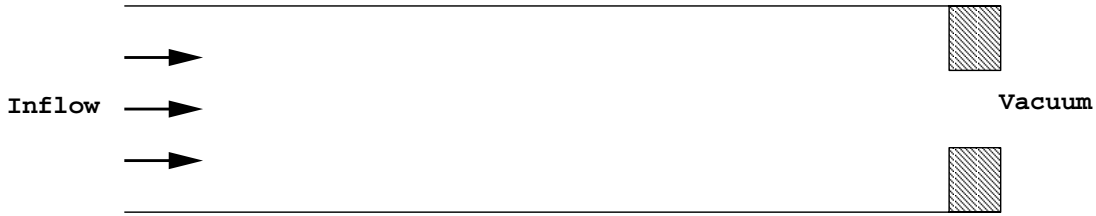


Figure 2: Geometry of the flow to be computed

- If the rough approximation is not accurate (this is the case at phase changes), the solution is found using a Gauss-Seidel method. At each iteration the following system is solved:

$$\delta\rho_j^{k+1} + a_j\delta P_{j-1}^{k+1} + b_j\delta P_j^{k+1} + c_j\delta P_{j+1}^k = RHS(j) \quad (49)$$

This system is initialised with the results of the first substep. For each point the solution is calculated using a method of dichotomy on the density.

- (4) Find  $m^{n+1}$  from equations (32) and (33).
- (5)  $T^{n+1}$ ,  $\rho^{n+1}$  and  $\chi^{n+1}$  the vapour fraction at equilibrium are computed from the thermodynamic model and the dryness equation.
- (6) Determine  $U^{n+1}$  from the momentum and the density.

## 6 PREDICTIONS OF HYDRAZINE VENTING

### 6.1 Flow configuration

In order to predict the flow behaviour, simulations of the end part of the vent line have been performed. The configuration to be computed is presented in figure 2. It is a pipe with a length of 20 cm and an inner diameter equal to half an inch (11.4 mm), at the ejection there is a an hole of 5.2 mm diameter. The mesh consists of a uniform coarse mesh of 40 cells over 16 cm, then a stretched zone of 28 cells over 32 mm and finally an uniform fine mesh of 20 cells over 4 mm. The ratio between the lengths of two consecutive cells of the stretched part is equal to 0.9. Several meshes have been applied for the simulations and the use of finer meshes was not found to influence the numerical results. The area jump is located in between a momentum point and a pressure point.

The inlet temperature is equal to 300 K for single-phase calculations and to 307 K for two-phase predictions. The mass-flow-rates are those given in table 3. The pressure imposed at the outlet is equal to 1 mbar for single-phase flows and to 16 mbar for the two-phase simulations. This value is the saturation pressure of the spray at equilibrium

Case	Velocity (m/s)	Mass flow rate (kg/s)	Tank pressure (bar)
1	4.11	0.42	6
2	5.58	0.57	12
3	8.23	0.84	25

Table 3: Conditions of the experimental study conducted by Foucaud [11]

Case	Calc. pressure (bar)	Exp. pressure (bar)
1	4.18	4.33
2	7.71	8.
3	16.82	17.

Table 4: Injection pressures calculated here and measured by Foucaud [11] for the different test cases

measured by Foucault [11] in a test chamber at ONERA.

The results have been obtained after 10000 time steps. They correspond to a steady flow for single-phase predictions. For two-phase predictions the convergence is not reached due to the thermodynamic model sensitivity to numerical perturbations. For the computed case the value of the residus taken as the maximum of  $|e_j^{n+1} - e_j^n|$  is equal to 0.0281. The CFL number (defined by  $CFL = U\Delta t/\Delta x$ ) used for the calculations is equal to 0.95 in single-phase flows and to 0.6 in two-phase calculations.

## 6.2 Single-phase flow

The three cases of table 3 have been computed. In order to validate the numerical results the computed injection pressures have been compared to those measured by Foucaud [11]. Table 4 shows that the predicted values fit very well with the experimental data. For each case the differences are very small, less than 0.3 bar. This agreement indicates that the quasi one-dimensional approach is capable to describe the global pressure drop along the pipe.

In figure 3 the pressure drop predicted for case 1 is presented. More than 80 % of the pressure decrease is located at the area change. Upstream of the area change, the pressure decreases smoothly due to friction. For the temperatures considered, the saturation pressure of hydrazine is around 20 mbar. Comparisons between the calculated pressure and the saturation pressure show that conditions for vaporization are reached near the exit. Figure 4 shows a zoom of the pressure distribution near the exit. The pressure reaches the saturation pressure at 0.3 mm from the outlet. This indicates that the liquid flashing is located at the exit, therefore the quantity of vapour inside the pipe should be small and the approach selected for the two-phase modelling valid.

In figure 5 the momentum distribution along the pipe is plotted for a tank pressure of 6 bar. For the two other test cases this quantity has exactly the same behaviour. The

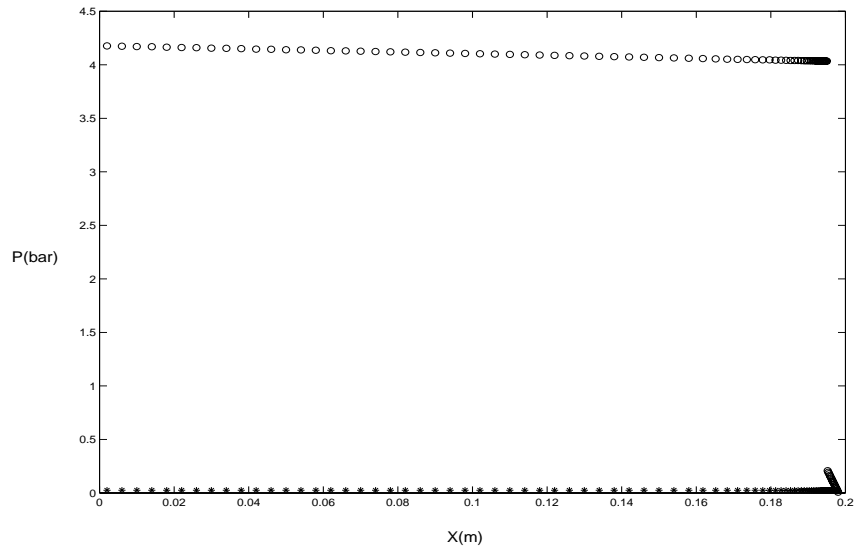


Figure 3: Pressure distribution (in bar) along the pipe for the case 1 (tank pressure of 6 bar): o o o calculated pressure; \* \* \* saturation pressure

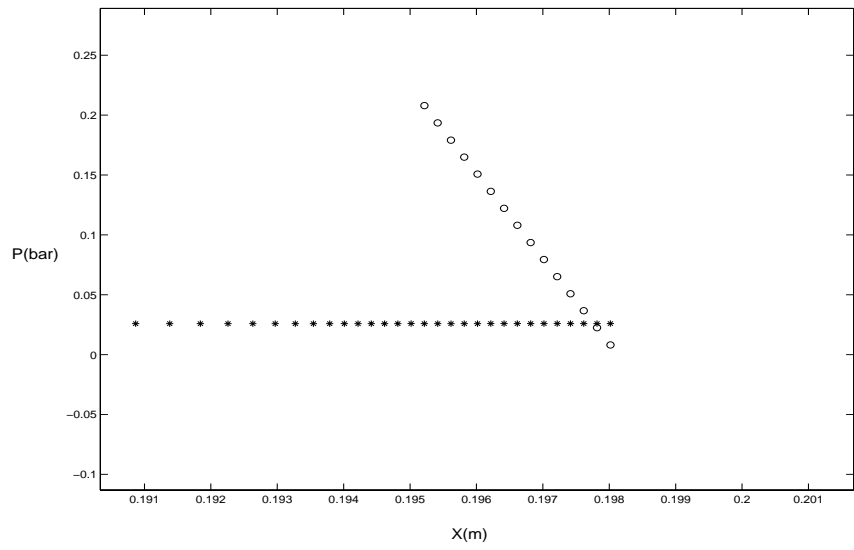


Figure 4: Zoom of the pressure distribution near the exit for the case 1: o o o calculated pressure; \* \* \* saturation pressure

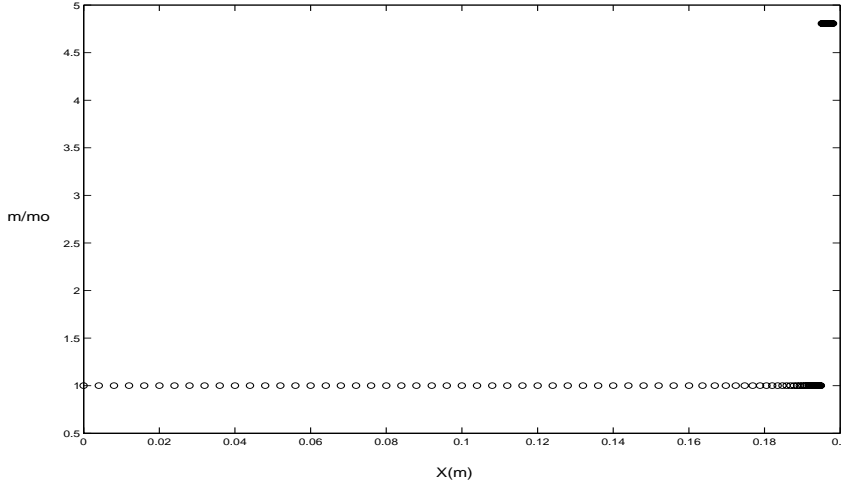


Figure 5: Momentum distribution along the pipe for case 1 (the momentum is non-dimensionalised by the inlet momentum, here  $m_o$  is equal to  $m_{left}$ )

momentum is constant upstream of the area change. In absence of phase change the fluid density remains nearly constant and as the cross-section area does not change there is no reason for momentum variations. This correspond to the conservation of the mass-flow-rate. This shows that the numerical scheme is applicable to the prediction of flows in geometries characterized by abrupt area changes.

The distribution of the internal energy for the case 3 is plotted in figure 6. There is a linear evolution upstream of the area change. Then, an increase occurs due to the singular term for the friction effects at the section change. This term corresponds to the multi-dimensional friction effects. After the increase of the internal energy the first point upstream of the area change is isolated. The correction term for the friction effects at the area change (see Reynier et al [13]) is distributed over the two adjacent pressure cells. This explains the presence of this point. Downstream of this location, the growth of the internal energy is linear due to a constant friction in the restricted part of the geometry.

The numerical results put in evidence a quasi constant density along the pipe. For the three test cases, the density decreases by less than 0.2 %. This result is in agreement with the thermodynamic which considers the liquid as a nearly incompressible fluid. The numerical results for the temperature like those for the density do not show large variations of this quantity. From the inlet to the outlet the variation of the temperature is lower than 0.2 K therefore the temperature can be considered as quasi constant along the pipe.

### 6.3 Two-phase flow

The case 1 of table 3 has been calculated with and without thermodynamic equilibrium. It is for this case that the saturation pressure is reached the farthest from the outlet. The

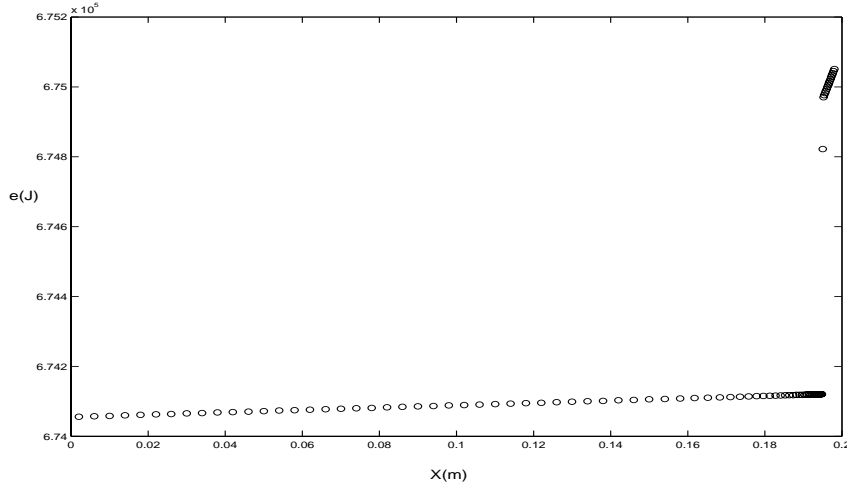


Figure 6: Distribution of the internal energy along the pipe for the case 3

calculations at equilibrium did not allow the prediction of a two-phase flow. This seems to be due to a high sensitivity of the thermodynamic model to numerical perturbations. Therefore, non-equilibrium calculations have been performed without using the second step of the pressure correction (this mean the Gauss-Seidel iteration coupled with a dichotomy). This non-equilibrium approach permits the predictions of a two-phase flow at the end of the pipe.

The axial distribution of the dryness fraction plotted in figure 7 indicates that the liquid flashing is located at the exit. As a consequence the quantity of vapour predicted inside the pipe is small. The numerical results indicate a void fraction equal to 0.08 at the exit. This is the limit of the validity of the mixture model. This result has to be compared with the experiments performed by Foucaud [11]. They establish the presence of some bubbles at the outlet but without much vaporization of the liquid. In the present study it seems that the numerical predictions overestimate the void fraction inside the pipe. This can be due to the not complete convergence of the calculation. Another way to improve the reliability of the simulations would be the use of a function for  $\theta_\chi$  has done by Downar-Zapolski [18] and Veneau [3].

The axial distribution of the density (see figure 8) shows, like for the single-phase simulations, a quasi constant density along the main part of pipe. Then, as soon as the vaporization process begins the density drops very rapidly. At the end of the pipe the density has decreased by 5 % which is much more than for the single-phase calculations.

Figure 9 represents the distribution of the temperature along the pipe. The results show a quasi constant temperature increasing slowly in the first part of the geometry. Then, some variations occurs at the end of the pipe. The behaviour of the temperature for the two-phase computations is close to the one observed in single-phase flows. This show

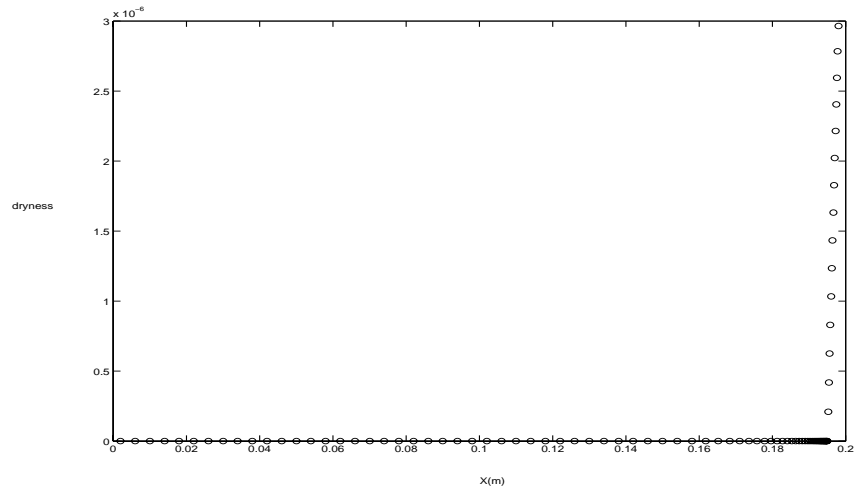


Figure 7: Distribution of the dryness fraction along the pipe for the case 1

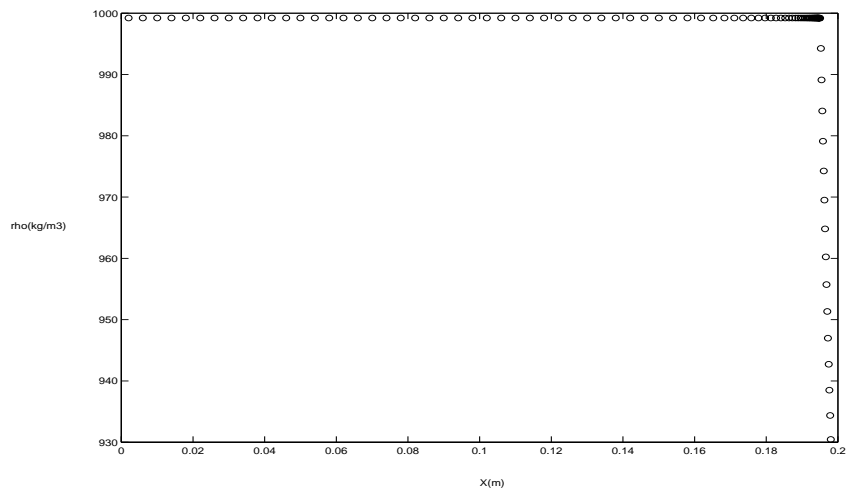


Figure 8: Density distribution along the pipe for the case 1

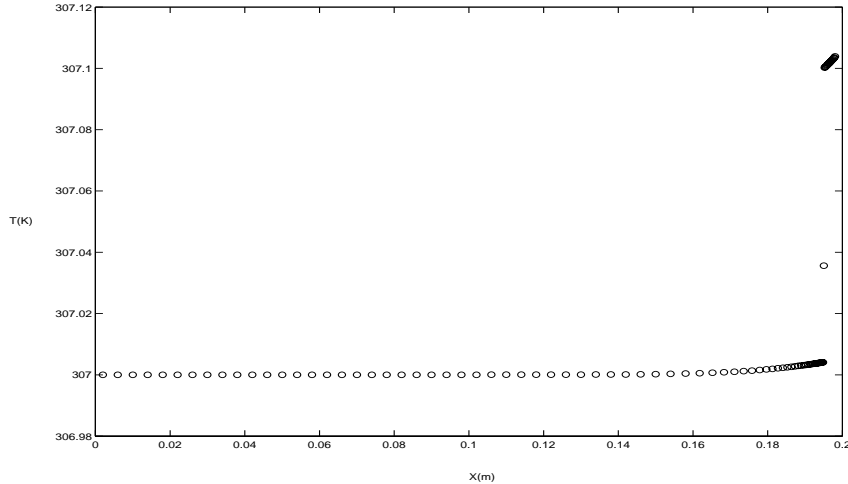


Figure 9: Temperature distribution along the pipe for the case 1

that even in presence of vaporization (at least for a low dryness fraction) the variations of temperature are not important (less than 0.5 K here). This indicates that a freezing of the liquid inside the pipe is avoided for the tank pressure range considered. Therefore, with the clogging of the pipe with the used final device should be not possible.

## 7 Conclusions

The developed method has been successfully applied to the prediction of liquid depressurization. The numerical scheme uses a staggered and a pressure correction. This algorithm has been coupled to a nonlinear two-phase thermodynamic model for hydrazine. This approach has been validated using experimental data and has simulated the behaviour of hydrazine during strong depressurization.

The single-phase predictions in the last part of the SCA device shows that conditions for vaporization are encountered inside the outlet. Two-phase predictions put in evidence that a small part of hydrazine should be vapourized. This result agrees with experimental investigations which show the presence of some bubbles at the outlet but without a lot of liquid vaporization. It seems that the predictions overestimate the void fraction inside the pipe. This could be due to a high sensitivity of the thermodynamic model to numerical perturbations or to the use of a constant instead of a function for the relaxation term. The numerical results do not put in evidence strong variations of temperature at the pipe exit. Therefore, the risk of clogging during the venting of hydrazine into space is avoided for the range of tank pressure considered.

The authors are grateful to Drs. Eric Hervieu and Hervé Lemonnier from the Centre d'Etudes Nucléaires de Grenoble for their valuable discussions and contributions on liquid

depressurization. We would like to thank also Ms. Martina De Serio from University of Bari for the assistance provided on thermodynamic and Dr. Richard Schwane from the European Space Agency for his helpful comments on numerical methods.

## REFERENCES

### References

- [1] M. Zeigerson-Katz and E. Sher, Spray: formation by flashing of a binary mixture: a parametric study. *Atomization and Sprays*, **8**, 255–266 (1998).
- [2] R. Curtelin, *Décompression d'un réservoir de propane liquéfié*, Ph. D. thesis, Ecole Centrale Paris (1991).
- [3] T. Veneau, *Etude expérimentale et modélisation de la décompression d'un réservoir de stockage de propane*, Ph. D. thesis, INP Grenoble (1995).
- [4] E. Hervieu and T. Veneau, Experimental determination of the droplet size and velocity distributions at the exit of the bottom discharge pipe of a liquefied propane storage tank during a sudden blowdown. *J. Loss Prev. Process Ind.*, **9(6)**, 413–425 (1996).
- [5] R.T. Neher, Saturn S-IVB continuous vent system for propellant control during parking orbit. In: *Proc. of 8<sup>th</sup> Space Congress Technology Today and Tomorrow*, Cocoa Beach, Florida, April 19–23, 4-17–4-25, (1971).
- [6] C.P. Pike, D.J. Knecht, R.A. Viereck, E. Murad, I.L. Kofski, M.A. Maris, N.H. Tran, G. Ashley, L. Twist, M.E. Gersh, J.B. Elgin, A. Berk, A.T. Stair, J.P. Bagian and J.F. Buchli, Release of liquid water from the space shuttle. *Geophysical Research Letters*, **17(2)**, 139–142 (1990).
- [7] I.L. Kofski, D.L.A. Rall, M.A. Maris, N.H. Tran, E. Murad, C.P. Pike, D.J. Knecht, R.A. Viereck, A.T. Stair and A. Setayesh, Phenomenology of a water venting in low earth orbit. *Acta Astronautica*, **26(5)**, 325–347 (1992).
- [8] D. Giordano and M. De Serio, Thermodynamic model of hydrazine with account for liquid-vapour phase change. *In preparation*.
- [9] H. Bijl and P. Wesseling, A unified method for computing incompressible and compressible flows in boundary-fitted coordinates. *J. Comp. Physics*, **141**, 153–173 (1998).
- [10] F.H. Harlow and J.E. Welch, Numerical calculation of time-dependent viscous incompressible flow of fluid with free surface. *Phys. Fluids*, **8(12)**, 2182–2189 (1965).

- [11] R. Foucaud, Passivation du système de contrôle d'attitude: Etude expérimentale du dispositif d'éjection prévu pour le vol 503. *Procès verbal de réalisation d'essais*, **RF 1/5400.37**, DMAE, ONERA (1998).
- [12] A.K. Jain, Accurate explicit equation for friction factor. *ASCE, J. Hydraulics Div.*, **102**, 674–677 (1976).
- [13] P. Reynier, P. Wesseling, L. Marraffa and D. Giordano, Computation of liquid hydrazine depressurization with a Mach-uniform staggered scheme, *submitted to Flow, Turbulence and Combustion*.
- [14] Z. Bilicki, D. Kardas and E.E. Michaelides, Relaxation models for wave phenomena in liquid-vapor bubble flow in channels, *J. Fluids Eng.*, **120**, 369–377 (1998).
- [15] K. Minemura, T. Uchiyama, S. Shoda and K. Egashira, Prediction of Air-Water two-phase flow performance of a centrifugal pump based on one-dimensional two-fluid model, *J. Fluids Eng.*, **120**, 327–334 (1998).
- [16] Z. Bilicki, R. Kwidinski & S.A. Mohammadein, Evaluation of the relaxation time of heat and mass exchange in the liquid-vapour bubble flow, *Int. J. of Heat Transfer*, **39(4)**, 753–759 (1996).
- [17] P. Reynier, L. Marraffa, P. Wesseling and G. Segal, Modelling and numerical simulation of Ariane 5 SCA venting, *ESA Working Paper*, **2076** (2000).
- [18] P. Downar-Zapolski, Z. Bilicki, L. Bolle and J. Franco, The nonequilibrium relaxation model for one-dimensional flashing liquid flows, *Int. J. of Multiphase Flow*, **22**, 473–483 (1996).